

# Landau damping of surface plasmons in metal nanostructures

Tigran V. Shahbazyan

*Department of Physics, Jackson State University, Jackson, MS 39217 USA*

We develop a quantum-mechanical theory for Landau damping of surface plasmons in metal nanostructures of arbitrary shape. We show that the electron surface scattering, which facilitates plasmon decay in small nanostructures, can be incorporated into the metal dielectric function *on par* with phonon and impurity scattering. The derived surface scattering rate is determined by the local field polarization relative to the metal-dielectric interface and is highly sensitive to the system geometry. We illustrate our model by providing analytical results for surface scattering rate in some common shape nanostructures. Our results can be used for calculations of hot carrier generation rates in photovoltaics and photochemistry applications.

## I. INTRODUCTION

Surface plasmons are collective electron excitations that provide unprecedented means for energy concentration, conversion, and transfer at the nanoscale [1–3]. Plasmons can be resonantly excited in metal-dielectric nanostructures giving rise to strong oscillating local fields that underpin numerous plasmon-enhanced spectroscopy phenomena, including surface-enhanced Raman scattering [4], plasmon-enhanced fluorescence and energy transfer [5], or plasmonic laser (spaser) [6]. Among key characteristics that impact many plasmonics applications [7–10] is the plasmon lifetime, which, depending on the plasmonic system size, is governed by several decay mechanisms [11–15]. While in large systems, the plasmon lifetime is mostly limited by radiation [16], in systems with characteristic size  $L < c/\omega$ , where  $c$  and  $\omega$  are, respectively, the light speed and frequency, the dominant decay mechanism is excitation of electron-hole ( $e$ - $h$ ) pairs by the plasmon local field accompanied by phonon and impurity scattering or, for small systems, surface scattering [17]. Recently, plasmon decay into  $e$ - $h$  pairs has attracted intense interest as a highly efficient way of hot carrier generation and transfer across the interfaces with applications in photovoltaics [18–27] and photochemistry [28–32]. Plasmon-assisted hot carrier generation is especially efficient in smaller plasmonic systems, where light scattering is relatively weak and extinction is dominated by resonant plasmon absorption. In such systems, carrier excitation is enhanced due to strong surface scattering that provides a new momentum relaxation channel [17].

Surface-assisted plasmon decay (Landau damping) has been extensively studied experimentally [33–43] and theoretically [44–59] since the pioneering paper by Kawabata and Kubo [44], who have shown that, for a spherical particle of radius  $a$ , the surface scattering rate is  $\gamma_{sp} = 3v_F/4a$ , where  $v_F$  is the electron Fermi velocity. In subsequent quantum-mechanical studies carried within random phase approximation (RPA) [45–51] and time-dependent local density approximation (TDLDA) [52–59] approaches, a more complicated picture has emerged involving the role of confining potential and nonlocal effects. These are dominant at the spatial scale  $\xi_{nl} = v_F/\omega$  that defines the characteristic length for nonlocal effects

[60, 61] (e.g., for noble metals,  $v_F/\omega < 1$  nm in the plasmon frequency range), whereas for larger systems with  $L \gg v_F/\omega$  (i.e., several nm and larger), they mainly affect the overall magnitude of  $\gamma_{sp}$ , while preserving intact its size dependence [56, 58]. The latter implies that in a wide size range  $v_F/\omega \ll L \ll c/\omega$ , which includes most plasmonic systems used in applications, the detailed structure of electronic states is unimportant, and the confinement effects can be reasonably described in terms of electron surface scattering, which can be incorporated, along with phonon and impurity scattering, in the metal dielectric function  $\varepsilon(\omega) = \varepsilon'(\omega) + i\varepsilon''(\omega)$ . Here, we adopt the Drude dielectric function  $\varepsilon(\omega) = \varepsilon_i(\omega) - \omega_p^2/\omega(\omega + i\gamma)$ , where  $\varepsilon_i(\omega)$  describes interband transitions,  $\omega_p$  is the plasma frequency, and  $\gamma$  is the scattering rate. Thus, it is expected that, for systems in the above size range, the scattering rate should be modified as  $\gamma = \gamma_0 + \gamma_s$ , where  $\gamma_0$  is the bulk scattering rate and  $\gamma_s$  is the *surface scattering rate*. In particular, the standard expression, in terms of metal dielectric function, for the plasmon decay rate [3],

$$\Gamma = 2\varepsilon''(\omega) \left[ \frac{\partial \varepsilon'(\omega)}{\partial \omega} \right]^{-1}, \quad (1)$$

should describe plasmon damping due to *both* bulk and surface-assisted processes if surface-modified  $\varepsilon(\omega)$  is used instead. For example, for  $\omega$  well below the onset of interband transitions, the rate (1) coincides with (modified) Drude scattering rate:  $\Gamma \approx \gamma = \gamma_0 + \gamma_s$ .

The major roadblock in the way of carrying this program forward has so far been the lack of any quantum-mechanical model for evaluation of  $\gamma_s$  in a nanostructure of *arbitrary* shape. Due to the complexity of electronic states in general-shape confined systems, calculations of  $\gamma_s$  were performed, within RPA [44–51] and TDLDA [52–59] approaches, only for some simple (mostly spherical) geometries. For general shape systems, the surface scattering rate was suggested, within the *classical scattering* (CS) model [62–66], in the form  $\gamma_{cs} = Av_F/L$ , where  $L$  is interpreted as the ballistic scattering length in a classical cavity, while the phenomenological constant  $A$  accounts for the effects of surface potential, electron spillover, and dielectric environment. However, the unreasonably wide range of measured  $A$  ( $0.3 \div 1.5$  for spher-

ical particles [17]) raised questions about the CS model validity [67], while recent measurements of plasmon spectra in nanoshells [38], nanoprisms [41], nanorods [42], and nanodisks [43] revealed significant discrepancies with its predictions. Furthermore, the CS approach is questionable on physical grounds as well since it involves carrier scattering across the entire system even for  $L \gg v_F/\omega$ , i.e., when the nonlocal effects are expected to be weak.

On the other hand, surface scattering should depend sensitively on the local fields accelerating the carriers towards the metal-dielectric interface. This dependence was, in fact, masked in all previous quantum-mechanical studies of simple-shape systems [44–59], where a specific functional form of the local field, appropriate for the given geometry, was adopted, while it is completely missing in the CS approach. Moreover, for the most widely studied spherical geometry, the local field is uniform inside the particle (apart from surface effects), which further obscured its importance. Note, however, that our recent RPA calculations of the surface plasmon lifetime in spherical metal nanoshells with dielectric core [68] revealed the crucial role of local fields; for thin shells, the field is pushed out of the metal region, resulting in a reduction of the plasmon decay rate. This result contrasts sharply with the CS model predictions but, in fact, is consistent with the measured light-scattering spectra of single nanoshells [38]. Furthermore, recent measurements of plasmon spectra in nanorods and nanodisks revealed strong sensitivity of plasmon modes' linewidth to the local field polarization relative to the system symmetry axis [43]. For general-shape systems, the local field orientation relative to the interface can strongly affect the surface scattering rate, and, therefore, must be properly accounted for in any consistent theory of surface-assisted plasmon decay.

In this paper, we present a quantum-mechanical theory for surface-assisted  $e$ - $h$  pair excitation by alternating local electric field  $\mathbf{E}e^{-i\omega t}$  in metal nanostructures of general shape. We note that intraband absorption of energy  $\hbar\omega$  takes place in a region of size  $v_F/\omega$  (see Fig. 1) and, therefore, can be viewed as a *local* process in systems with characteristic size  $L \gg v_F/\omega$ . We show that, within RPA, surface scattering can be included into the Drude dielectric function by modifying the scattering rate as  $\gamma = \gamma_0 + \gamma_s$ . We derive the surface scattering rate  $\gamma_s$  as

$$\gamma_s = A v_F \frac{\int dS |E_n|^2}{\int dV |\mathbf{E}|^2}, \quad (2)$$

where  $E_n$  is the local field component *normal* to the interface and the integrals are carried over the metal surface (numerator) and volume (denominator). The constant  $A$  has the value  $A = 3/4$  for hard-wall confining potential, but can be adjusted to account for surface and nonlocal effects. The full plasmon decay rate, including bulk and surface contributions, has still the form (1), but with modified  $\varepsilon(\omega)$  that now includes the surface scattering rate (2). Surface scattering is highly sensitive to the local field polarization relative to the metal-dielectric interface,

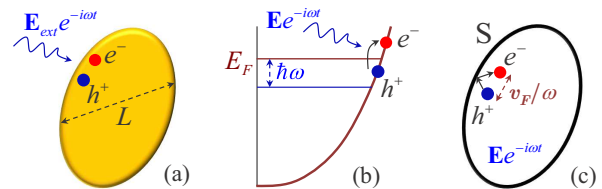


FIG. 1. Schematics for surface-assisted excitation of an  $e$ - $h$  pair with energy  $\hbar\omega$ . (a) An external optical field incident on a metal nanostructure of characteristic size  $L$ , (b) excites a surface plasmon that decays into an  $e$ - $h$  pair, (c) accompanied by momentum relaxation via carrier surface scattering in a small region of size  $v_F/\omega \ll L$ .

leading to distinct rates for different plasmon modes, as we illustrate here for some common geometries.

The paper is organized as follows. In Sec. II, we outline our approach to plasmon Landau damping in metal nanostructures. In Sec. III, we derive an explicit expression for surface-assisted absorbed power and the corresponding scattering rate in systems of arbitrary shape. In Sec. IV, we present analytical and numerical results for surface scattering rates in some common nanostructures. In Sec. V, we discuss the effect of confining potential profile on the surface scattering rate, and the Appendices detail some technical aspects of our calculations.

## II. DECAY RATE OF SURFACE PLASMONS IN METAL NANOSTRUCTURES

In this section, we outline our approach to calculation of the plasmon decay rate for a metal nanostructure embedded in dielectric medium. For simplicity, we restrict ourselves by metal structures occupying some volume  $V$  with a single surface  $S$ , so that the local dielectric function  $\varepsilon(\omega, \mathbf{r}) = \varepsilon'(\omega, \mathbf{r}) + i\varepsilon''(\omega, \mathbf{r})$  equals  $\varepsilon(\omega)$  and  $\varepsilon_d$  in the metal and dielectric regions, respectively. For systems with characteristic size  $L \ll c/\omega$ , the retardation effects are unimportant, and plasmon modes are determined by the Gauss law  $\nabla \cdot [\varepsilon'(\omega_l, \mathbf{r}) \mathbf{E}_l(\mathbf{r})] = 0$ , where  $\mathbf{E}_l(\mathbf{r})$  is the slow component of plasmon local field and  $\omega_l$  is the plasmon mode frequency. For brevity, we omit the mode index  $l$  hereafter. The general expression for plasmon decay rate  $\Gamma$  has the form [69]

$$\Gamma = \frac{Q}{U}, \quad (3)$$

where  $U$  is the mode energy [70],

$$U = \frac{\omega}{16\pi} \frac{\partial \varepsilon'(\omega)}{\partial \omega} \int dV |\mathbf{E}|^2, \quad (4)$$

and  $Q$  is the absorbed power (loss function)

$$Q = \frac{\omega}{2} \text{Im} \int dV \mathbf{E}^* \cdot \mathbf{P}. \quad (5)$$

Here,  $\mathbf{P}(\mathbf{r})$  is the electric polarization vector and the star stands for complex conjugation. In the classical (local)

picture, the polarization vector is proportional to the local field,  $\mathbf{P}_{loc}(\mathbf{r}) = \mathbf{E}(\mathbf{r})[\varepsilon(\omega, \mathbf{r}) - 1]/4\pi$ , yielding the absorbed power due to the bulk processes [70]

$$Q = \frac{\omega \varepsilon''(\omega)}{8\pi} \int dV |\mathbf{E}|^2, \quad (6)$$

which, along with the mode energy (4), leads to the standard form (1) of the plasmon damping rate.

Surface contribution to the absorbed power,  $Q_s$ , comes from the momentum relaxation channel provided by carrier scattering from the metal-dielectric interface. Since surface scattering introduces nonlocality,  $Q_s$  must be evaluated microscopically. The general expression for  $Q_s$  can be obtained by relating  $\mathbf{P}(\mathbf{r})$  to the electron polarization operator  $P(\omega; \mathbf{r}, \mathbf{r}')$  via the induced charge density:

$$\rho(\mathbf{r}) = e \int d\mathbf{r}' P(\mathbf{r}, \mathbf{r}') \Phi(\mathbf{r}') = -\nabla \cdot \mathbf{P}(\mathbf{r}), \quad (7)$$

where local potential  $\Phi(\mathbf{r})$  is defined as  $e\mathbf{E}(\mathbf{r}) = -\nabla\Phi(\mathbf{r})$  ( $e$  is the electron charge). With the help of Eq. (7), integration of Eq. (5) by parts yields

$$Q_s = \frac{\omega}{2} \text{Im} \int dV dV' \Phi^*(\mathbf{r}) P(\omega; \mathbf{r}, \mathbf{r}') \Phi(\mathbf{r}'), \quad (8)$$

where  $P(\omega; \mathbf{r}, \mathbf{r}')$  includes only the electronic contribution, i.e., without phonon and impurity scattering effects. Within RPA,  $P(\omega; \mathbf{r}, \mathbf{r}')$  is replaced by the polarization operator for noninteracting electrons [71], yielding

$$Q_s = \pi\omega \sum_{\alpha\beta} |M_{\alpha\beta}|^2 [f(\epsilon_\alpha) - f(\epsilon_\beta)] \delta(\epsilon_\alpha - \epsilon_\beta + \hbar\omega), \quad (9)$$

where  $M_{\alpha\beta} = \int dV \psi_\alpha^* \Phi \psi_\beta$  is the transition matrix element of local potential  $\Phi(\mathbf{r})$  calculated from the wave functions  $\psi_\alpha(\mathbf{r})$  and  $\psi_\beta(\mathbf{r})$  of electron states with energies  $\epsilon_\alpha$  and  $\epsilon_\beta$  separated by  $\hbar\omega$ ,  $f(\epsilon)$  is the Fermi distribution function, and spin degeneracy is accounted for.

In terms of  $Q_s$ , the surface-assisted contribution to the plasmon decay rate, i.e., the Landau damping (LD) rate, has the form

$$\Gamma_s = \frac{Q_s}{U}, \quad (10)$$

where  $U$  is given by Eq. (4). Note that often in the literature,  $\Gamma_s$  is identified with the standard first-order transition probability rate, given by the expression similar to Eq. (9) but divided by the factor  $\hbar\omega/2$ . We stress that in a system with dispersive dielectric function, where the mode energy is  $U$  rather than  $\hbar\omega$  [70], the standard transition rate must be rescaled by the factor  $\hbar\omega/2U$  [69].

Calculation of  $Q_s$  (and, hence, of  $\Gamma_s$ ) hinges on the transition matrix element  $M_{\alpha\beta}$ , which has so far been evaluated, either analytically or numerically, only for several simple geometries permitting separation of variables [44–58, 68]. For general-shape systems, evaluation of  $M_{\alpha\beta}$  presents an insurmountable challenge of finding, with a good accuracy, the three-dimensional electron wave functions oscillating rapidly, with the Fermi

wavelength period  $\lambda_F$ , on the system size scale  $L \gg \lambda_F$ . However, as we demonstrate in the following section, this difficulty can be bypassed and even turned into an advantage as  $Q_s$  is derived in a closed form for any nanostructure larger than the nonlocality scale, i.e., for  $L \gg v_F/\omega$ .

### III. ABSORBED POWER AND SURFACE SCATTERING RATE

In this section, we derive the surface contribution  $Q_s$  to the absorbed power due to  $e$ - $h$  pair excitation by alternating local field  $\mathbf{E}e^{-i\omega t}$  created in the metal either by plasmons or as a response to an external field.

We start with the transition matrix element  $M_{\alpha\beta} = \int dV \psi_\alpha^* \Phi \psi_\beta$ , where  $\psi_\alpha(\mathbf{r})$  is the eigenfunction of the Hamiltonian  $H = -(\hbar^2/2m)\Delta$  for an electron with energy  $\epsilon_\alpha$  in a hard-wall cavity (this approximation is discussed later). We consider the case when excitation energy  $\hbar\omega$  is much larger than the electron level spacing, so that, in the absence of phonon and impurity scattering, the electron transition to the state  $\psi_\beta(\mathbf{r})$  with energy  $\epsilon_\beta = \epsilon_\alpha + \hbar\omega$  requires momentum transfer to the interface. A direct evaluation of  $M_{\alpha\beta}$ , so far carried out only for some simple geometries [44–58, 68], requires the knowledge of  $\psi_\alpha$  in the entire system volume. We note, however, that for a typical plasmon frequency  $\hbar\omega \ll E_F$ , where  $E_F$  is the Fermi energy in the metal, the momentum transfer  $q \sim \hbar\omega/v_F$  takes place in a region of size  $\xi_{nl} \sim \hbar/q \sim v_F/\omega$ , so that, for characteristic system size  $L \gg v_F/\omega$ , the  $e$ - $h$  pair excitation takes place in a close proximity to the interface (see Fig. 1). It is our observation that, for an electron in a hard-wall cavity, the boundary contribution to  $M_{\alpha\beta}$  can be extracted as a surface integral of the form,

$$M_{\alpha\beta}^s = \frac{-e\hbar^4}{2m^2\epsilon_{\alpha\beta}^2} \int dS [\nabla_n \psi_\alpha(\mathbf{s})]^* E_n(\mathbf{s}) \nabla_n \psi_\beta(\mathbf{s}), \quad (11)$$

where  $\nabla_n \psi_\alpha(\mathbf{s})$  is the wave-function normal derivative at a surface point  $\mathbf{s}$ ,  $E_n(\mathbf{s})$  is the corresponding normal field component,  $\epsilon_{\alpha\beta} = \epsilon_\alpha - \epsilon_\beta$  is the  $e$ - $h$  pair excitation energy, and  $m$  is the electron mass. The derivation of Eq. (11) is given in Appendix A. Using the above matrix element, Eq. (9) can be recast as

$$Q_s = \frac{e^2 \hbar^4}{4\pi m^4 \omega^3} \iint dS dS' E_n(\mathbf{s}) E_n^*(\mathbf{s}') F_\omega(\mathbf{s}, \mathbf{s}'), \quad (12)$$

where  $F_\omega(\mathbf{s}, \mathbf{s}')$  stands for  $e$ - $h$  surface correlation function defined as

$$F_\omega(\mathbf{s}, \mathbf{s}') = \int d\epsilon f_\omega(\epsilon) \rho_{nn'}(\epsilon; \mathbf{s}, \mathbf{s}') \rho_{n'n}(\epsilon + \hbar\omega; \mathbf{s}', \mathbf{s}). \quad (13)$$

Here, the function  $f_\omega(\epsilon) = f(\epsilon) - f(\epsilon + \hbar\omega)$  restricts the electron initial energy to the interval  $\hbar\omega$  below  $E_F$ , and

$$\rho_{nn'}(\epsilon; \mathbf{s}, \mathbf{s}') = \nabla_n \nabla_n' \text{Im} G(\epsilon; \mathbf{s}, \mathbf{s}') \quad (14)$$

is the normal derivative of the electron cross density of states  $\rho(\epsilon; \mathbf{r}, \mathbf{r}') = \text{Im}G(\epsilon; \mathbf{r}, \mathbf{r}')$  at surface points, where

$$G(\epsilon; \mathbf{r}, \mathbf{r}') = \sum_{\alpha} \frac{\psi_{\alpha}(\mathbf{r})\psi_{\alpha}^*(\mathbf{r}')}{\epsilon - \epsilon_{\alpha} + i0} \quad (15)$$

is the Green function of a confined electron. Note that neither the Green function  $G(\epsilon; \mathbf{r}, \mathbf{r}')$  nor the correlation function  $F_{\omega}(\mathbf{s}, \mathbf{s}')$  can be evaluated with any reasonable accuracy for a general-shape cavity. However, an explicit expression for  $Q_s$  in terms of local fields can still be derived by exploiting the difference in the length scales characterizing electron and plasmon excitations. Namely, while the electron wave-functions oscillate with the Fermi wave length period  $\lambda_F$ , the local fields significantly change on the much larger system scale  $L \gg \lambda_F$ . Below we outline the main steps of our derivation of  $Q_s$  and refer to Appendix B for details.

First, we note that since excitation of an  $e$ - $h$  pair with energy  $\hbar\omega$  near the Fermi level takes place in a region of size  $v_F/\omega$ , the correlation function  $F_{\omega}(\mathbf{s}, \mathbf{s}')$  peaks in the region  $|\mathbf{s} - \mathbf{s}'| \lesssim v_F/\omega \ll L$  and rapidly oscillates outside of it (see below). On the other hand, in such a region, the local field  $E_n$  is nearly constant, i.e.,  $E_n(\mathbf{s}) \approx E_n(\mathbf{s}')$ , and so  $Q_s$  takes the form

$$Q_s = \frac{e^2 \hbar^4}{4\pi m^4 \omega^3} \int dS |E_n(\mathbf{s})|^2 \bar{F}_{\omega}(\mathbf{s}), \quad (16)$$

where  $\bar{F}_{\omega}(\mathbf{s}) = \int dS' F_{\omega}(\mathbf{s}, \mathbf{s}')$  is, for  $L \gg v_F/\omega$ , independent of the surface point  $\mathbf{s}$ .

Evaluation of  $\bar{F}_{\omega}$  is based upon multiple-reflection expansion for the electron Green function  $G(\epsilon; \mathbf{s}, \mathbf{s}')$  in a hard-wall cavity [72]. For  $L \gg \lambda_F$ , the direct and single-reflection paths provide the dominant contribution, while higher-order reflections are suppressed as powers of  $\lambda_F/L \ll 1$  (see Appendix B), and we obtain

$$\rho_{nn'}(\epsilon; \mathbf{s}, \mathbf{s}') = 2\nabla_n \nabla'_n \text{Im}G_0(\epsilon, \mathbf{s} - \mathbf{s}') \quad (17)$$

where

$$G_0(\epsilon, r) = \frac{m}{2\pi\hbar^2} \frac{e^{ik_{\epsilon}r}}{r}, \quad k_{\epsilon} = \frac{\sqrt{2m\epsilon}}{\hbar}, \quad (18)$$

is the free electron Green function, and factor 2 reflects equal contributions of direct and reflected paths at a surface point. It is now easy to see that, for  $\epsilon \sim E_F$  and  $\hbar\omega/E_F \ll 1$ , the integrand of Eq. (13) peaks in the region

$$|\mathbf{s} - \mathbf{s}'| \lesssim \frac{1}{k_{\epsilon+\hbar\omega} - k_{\epsilon}} \approx \frac{v_F}{\omega} \quad (19)$$

and rapidly oscillates outside of it. This sets up the length scale  $v_F/\omega$  for correlation function  $F_{\omega}(\mathbf{s}, \mathbf{s}')$  in Eq. (12) and leads to Eq. (16). The final step is to compute the normal derivatives in Eq. (17) which, for  $L \gg v_F/\omega$ , is accomplished by approximating the surface by the tangent plane at the surface point (see Appendix B), yielding

$$\bar{F}_{\omega} = \hbar\omega \frac{2m^4 E_F^2}{\pi\hbar^8}. \quad (20)$$

Substituting this  $\bar{F}_{\omega}$  into Eq. (16), we finally arrive at the surface contribution to the absorbed power

$$Q_s = \frac{e^2}{2\pi^2\hbar} \frac{E_F^2}{(\hbar\omega)^2} \int dS |E_n|^2 = \frac{3v_F}{32\pi} \frac{\omega_p^2}{\omega^2} \int dS |E_n|^2. \quad (21)$$

The above expression for the surface absorbed power  $Q_s$ , which is our central result, is valid for *any* metal nanostructure with characteristic size  $L \ll c/\omega$  in an alternating electric field with frequency  $\omega \gg v_F/L$ .

The surface contribution (21) should be considered in conjunction with the bulk contribution to the absorbed power. In fact, both contributions can be combined in the general expression (6) for absorbed power by modifying the scattering rate in the Drude dielectric function  $\epsilon(\omega) = \epsilon_i(\omega) - \omega_p^2/\omega(\omega + i\gamma)$  as  $\gamma = \gamma_0 + \gamma_s$ , where

$$\gamma_s = \frac{3v_F}{4} \frac{\int dS |E_n|^2}{\int dV |\mathbf{E}|^2}, \quad (22)$$

is the *surface scattering rate*. Then, the surface contribution  $Q_s$ , Eq. (21), is obtained as the first-order term in the expansion of full absorbed power  $Q$ , Eq. (6), over  $\gamma_s$ , implying that the surface scattering rate enters *on par* with its bulk counterpart into the metal dielectric function. While  $\gamma_s$  is independent of the local field strength, it does depend strongly on its *polarization* relative to the interface and, in fact, represents the *averaged* over the surface local scattering rate.

Finally, let us show that the full plasmon decay rate  $\Gamma$  due to *both* bulk and surface scattering is still given by the general expression (1), but with modified dielectric function  $\epsilon(\omega)$  that now includes the surface scattering rate (22). Indeed, using Eqs. (21) and (4), the surface contribution to  $\Gamma$ , i.e., the LD rate, takes the form

$$\Gamma_s = \frac{Q_s}{U} = \frac{2\omega_p^2 \gamma_s}{\omega^3} \left[ \frac{\partial \epsilon'(\omega)}{\partial \omega} \right]^{-1}. \quad (23)$$

The same expression is obtained by expanding Eq. (1) [with modified  $\epsilon(\omega)$ ] to the first order in  $\gamma_s$ . For  $\omega$  well below the interband transitions onset, the LD rate and surface scattering rate coincide,  $\Gamma_s \approx \gamma_s$ .

#### IV. EVALUATION OF SURFACE SCATTERING RATES FOR SPECIFIC GEOMETRIES

The strong polarization dependence of the surface absorbed power  $Q_s$  and surface scattering rate  $\gamma_s$  makes it possible to manipulate, in a wide range, the hot carrier excitation efficiency by realigning the electric field orientation [10]. This effect can be described by *surface enhancement factor*  $M$  defined as the ratio of the full absorbed power,  $Q = Q_b + Q_s$ , to the bulk one,  $Q_b$ . Within RPA, the enhancement factor takes a simple form  $M = 1 + \gamma_s/\gamma_0$ , i.e., it is completely determined by the surface scattering rate.

Using our model, surface scattering rates for nanostructure of arbitrary shape can be evaluated directly from the local fields, without further resorting to quantum-mechanical calculations. In this section, we employ our main result Eq. (22) to evaluate  $\gamma_s$  for some common structures: spherical particles, cylindrical wires, and spheroidal particles (nanorods and nanodisks).

We start with recasting the surface scattering rate (22) as the ratio of two surface integrals,

$$\gamma_s = \frac{3v_F}{4} \frac{\int dS |\nabla_n \Phi|^2}{\int dS \Phi^* \nabla_n \Phi}, \quad (24)$$

where the real part of the denominator is implied. This representation is especially useful for systems, whose shape permits separation of variables, and, as we show below, it yields *analytical* results for some common structures, such as nanorods and nanodisks, which so far eluded any attempts of quantum-mechanical evaluation of  $\gamma_s$ .

### A. Spherical particles and cylindrical wires

Let us first apply Eq. (24) to the simplest case of a sphere of radius  $a$ . In the quasistatic limit, the potentials inside the sphere are given by regular solutions of the Laplace equation,  $\Phi \propto r^l Y_{lm}(\hat{\mathbf{r}})$ , where  $r$  is the radial coordinate and  $Y_{lm}(\hat{\mathbf{r}})$  are the spherical harmonics ( $l$  and  $m$  are, respectively, the polar and azimuthal numbers). Then, a straightforward evaluation of Eq. (24) recovers the surface scattering rate for the  $l$ th mode [45]:

$$\gamma_{sp}^l = \frac{3lv_F}{4a}. \quad (25)$$

The same rate is obtained for the  $l$ th transverse mode in an infinite cylindrical nanowire of radius  $a$ .

### B. Nanorods and nanodisks

Nanorods and nanodisks are often modeled by prolate and oblate spheroids, respectively. Here we distinguish between longitudinal and transverse modes oscillating along the symmetry axis and within the symmetry plane, characterized, respectively, by semiaxes  $a$  and  $b$  (see Fig. 2). Using Eq. (24), the surface scattering rate for all modes can be found in an analytical form (see Appendix C), but here only the results for the dipole modes are presented. For a nanorod (prolate spheroid) with aspect ratio  $b/a < 1$ , we obtain the following rates for longitudinal and transverse polarizations, respectively:

$$\begin{aligned} \gamma_s^L &= \frac{3v_F}{4a} \frac{3}{2 \tan^2 \alpha} \left[ \frac{2\alpha}{\sin 2\alpha} - 1 \right], \\ \gamma_s^T &= \frac{3v_F}{4a} \frac{3}{4 \sin^2 \alpha} \left[ 1 - \frac{2\alpha}{\tan 2\alpha} \right], \end{aligned} \quad (26)$$

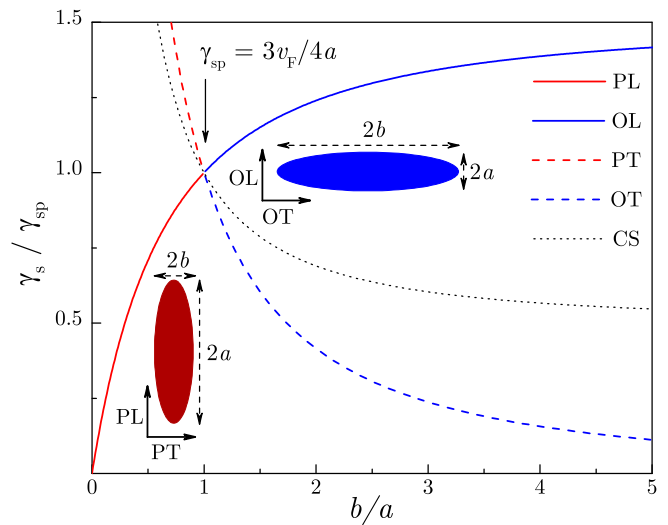


FIG. 2. Normalized surface scattering rates for prolate and oblate spheroids are shown with changing aspect ratio  $b/a$  along with the CS rate. Insets: Schematics of plasmon modes' polarizations.

where  $\alpha = \arccos(b/a)$  is the angular eccentricity. For a nanodisk (oblate spheroid) with  $b/a > 1$ , the rates (26) apply with  $\alpha = i \operatorname{arccosh}(b/a)$ . Note that the CS rate for a spheroidal particle is [65]

$$\gamma_{cs} = \frac{v_F S}{4V} = \frac{3v_F}{8a} \left( 1 + \frac{2\alpha}{\sin 2\alpha} \right). \quad (27)$$

### C. Numerical Results

Here we present calculated surface scattering rates for spheroidal particles as the system shape evolves, with changing aspect ratio  $b/a$ , from a needle to a pancake. In Fig. 2, we plot the rates (26) normalized by the dipole mode rate  $\gamma_{sp} = 3v_F/4a$  for spherical particle of radius  $a$ . At the sphere point  $a = b$ , the normalized rates for prolate and oblate spheroids continuously transition into each other (e.g., PL to OL and PT to OT), and depending on the mode polarization, exhibit dramatic differences in behavior with changing aspect ratio. The normalized rate for the PL mode *decreases* with reducing  $b/a$ , in sharp contrast to the CS rate, which shows the opposite trend. In the needle limit  $b/a \ll 1$ , the PL mode rate depends linearly on  $b$ ,

$$\gamma_s^{\text{PL}} \approx \frac{9\pi v_F b}{16a^2}, \quad (28)$$

while both the PT mode rate and CS rate are inversely proportional to  $b$ ,

$$\gamma_s^{\text{PT}} \approx \frac{9\pi v_F}{32b}, \quad \gamma_{cs} \approx \frac{3\pi v_F}{16b}. \quad (29)$$

The similar behavior  $\gamma_s^{\text{PT}}$  and  $\gamma_{cs}$  for  $b/a \ll 1$  originates the fact that random ballistic scattering is dominated by

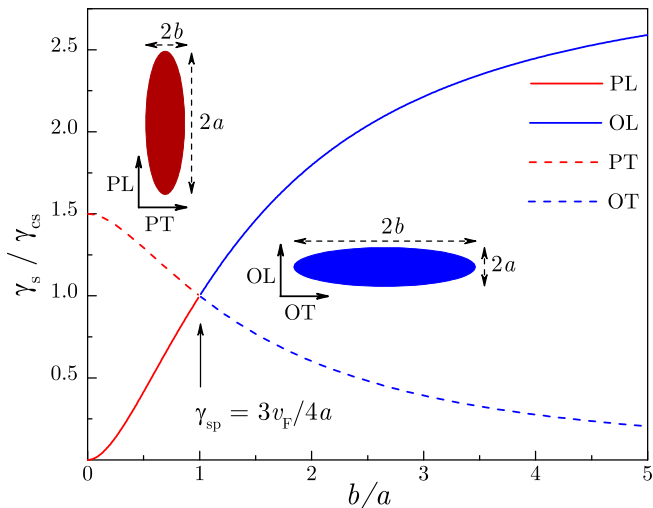


FIG. 3. Surface scattering rates for prolate and oblate spheroids normalized by the CS rate are shown with changing aspect ratio  $b/a$ .

the shortest system length. Note, however, that the former exceeds the latter ( $\gamma_s^{\text{PT}}/\gamma_{cs} \rightarrow 3/2$ ) since directional scattering is more efficient than random one.

For nanodisks ( $b/a > 1$ ), the above trends are reversed: With increasing  $b/a$ , as the nanodisk flattens, the normalized rates are increasing for the longitudinal (OL) mode and decreasing for the transverse (OT) mode (see Fig. 2). In the pancake limit  $b/a \gg 1$ , the OL mode rate and CS rate are dominated by the pancake height  $a$ , which is now the shortest length,

$$\gamma_s^{\text{OL}} \approx \frac{9v_F}{8a}, \quad \gamma_{cs} \approx \frac{3v_F}{8a}, \quad (30)$$

with their ratio  $\gamma_s^{\text{OL}}/\gamma_{cs} \rightarrow 3$ , while the OT mode rate exhibits a more complicated behavior:

$$\gamma_s^{\text{OT}} \approx \frac{9v_F a}{16b^2} \left[ \ln \left( \frac{2b}{a} \right)^2 - 1 \right]. \quad (31)$$

To highlight the role of the local fields in surface scattering, we show in Fig. 3 the evolution, with changing  $b/a$ , of  $\gamma_s$  for all modes, normalized by the CS rate  $\gamma_{cs}$ . Here, we have  $\gamma_s < \gamma_{cs}$  for the field polarization mostly tangential to the system boundary (PL and OT modes), and  $\gamma_s > \gamma_{cs}$  for mostly normal polarization (PT and OL modes). Note that recent measurements [43] in cylinder-shaped nanorods and nanodisks revealed strong polarization dependence of the plasmon spectrum linewidth.

## V. CONCLUSIONS

In conclusion, let us discuss the assumptions and approximations we made in deriving the surface scattering rate (2). First, we assumed that the metal nanostructure is characterized by a single metal-dielectric interface. Our model can be straightforwardly extended to systems

with two or more interfaces, such as, e.g., core-shell particles of various shapes or onion-like structures, by including each interface contribution in the matrix element  $M_{\alpha\beta}^s$  [see Eq. (11)]. Importantly, the surface contribution  $Q_s$  to the absorbed power, containing  $|M_{\alpha\beta}^s|^2$  [see Eq. (9)], will now include interference terms due to carrier scattering between the interfaces. For two interfaces that are sufficiently close to each other, such interference terms would lead to *coherent* oscillations (quantum beats), with the period  $v_F/\omega$ , of the surface scattering rate with changing interface separation. Such oscillations were recently identified and studied in detail for spherical metal nanoshells with dielectric core [68].

We considered systems with characteristic size  $L$  significantly larger than the nonlocality scale  $v_F/\omega$  [60, 61] (i.e., with  $L$  at least several nm large), and with electron level spacing much smaller than the optical energy  $\hbar\omega$ . Correspondingly, we disregarded quantum confinement effects that dominate optical response of small metal clusters. Specifically, the large electron level spacing in nanometer-sized clusters leads to oscillatory behavior of the resonance width [52, 53] (not to be confused with the above coherent oscillations [68]) that should be visible, e.g., in small aspect ratio behavior of  $\gamma_s$  in Figs. 2 and 3. Such effects are best described within the TDLDA approach [52–59] and are out of scope of this paper.

Finally, let us discuss the effect of realistic confining potential profile on the surface scattering rate. While the hard-wall approximation is often used for systems larger than several nm [44–51], recent TDLDA calculations for spherical particles indicate that, even for relatively large systems, deviations of the surface barrier from rectangular shape do affect the overall magnitude of the plasmon decay rate [55, 56, 58]. Importantly, the potential profile has distinct effects on the rapidly-oscillating electron wave-functions and slowly-varying plasmon local fields, which both determine the transition matrix element (11). While, within TDLDA, the Kohn-Sham wave functions are directly determined by the (self-consistent) confining potential, the local fields are, instead, defined solely by the induced charge density via the (screened) Coulomb potential and, therefore, depend on the confining potential indirectly. Hence, the *deviation* of  $E_n$  from its classical behavior across the interface is determined by the electron density spillover over the classical (hard wall) boundary [73], and, therefore, is largely *independent* of the system overall shape. Furthermore, recent TDLDA studies of relatively large (up to 10 nm) nanoparticles revealed [55, 56] that the main impact on plasmon linewidth comes precisely from the electron density tail and dielectric environment, implying that it is the plasmon local field near the interface, rather than electron wave functions, that chiefly determines the plasmon decay rate magnitude in real structures. We now note that we employed the hard-wall approximation *only* for evaluation of the  $e$ - $h$  correlation function (13), while retaining explicit local field dependence in the surface scattering rate. Therefore, for general shape systems,

the latter can still be obtained, in a good approximation, from Eq. (2) using the classical local fields, but with the constant  $A$  calculated self-consistently for some specific (e.g., spherical) system geometry, i.e.,  $A \approx 0.32$  [55, 56].

In summary, we developed a quantum-mechanical theory for Landau damping of surface plasmons in metal nanostructures of arbitrary shape. We derived an explicit expression for the surface scattering rate that can be included, *on par* with the bulk scattering rate, in the metal dielectric function. The rate is strongly dependent on the local field polarization, and is highly sensitive to the system geometry. Our results can be used for calculations of hot carrier generation rates in photovoltaics and photochemistry applications.

## ACKNOWLEDGMENTS

This work was supported in part by the National Science Foundation under Grant No. DMR-1610427 and No. HRD-1547754.

### Appendix A: Transition matrix element

To extract surface contribution to the matrix element

$$M_{\alpha\beta} = \int dV \psi_\alpha^* \Phi \psi_\beta, \quad (\text{A1})$$

we first apply the Hamiltonian  $H = -(\hbar^2/2m)\Delta$  to the wave function product as

$$\begin{aligned} \psi_\alpha^* \psi_\beta &= \frac{1}{\epsilon_{\alpha\beta}} (\psi_\beta H \psi_\alpha^* - \psi_\alpha^* H \psi_\beta) \\ &= \frac{\hbar^2}{2m\epsilon_{\alpha\beta}} \nabla_\mu (\psi_\alpha^* \nabla_\mu \psi_\beta - \psi_\beta \nabla_\mu \psi_\alpha^*), \end{aligned} \quad (\text{A2})$$

where  $\epsilon_{\alpha\beta} = \epsilon_\alpha - \epsilon_\beta$  is the excitation energy, and summation over repeating indices  $\mu = (x, y, z)$  is implied. After integrating by parts, the matrix element takes the form

$$M_{\alpha\beta} = \frac{e\hbar^2}{m\epsilon_{\alpha\beta}} \int dV \psi_\alpha^* (\nabla_\mu \psi_\beta) E_\mu, \quad (\text{A3})$$

where  $eE_\mu = -\nabla_\mu \Phi$  are the electric field components, and we used that  $\nabla_\mu E_\mu = 0$  inside the metal and  $\psi_\alpha$  vanish at the boundary  $S$ . Applying again the Hamiltonian  $H$  to Eq. (A3), we write

$$\begin{aligned} M_{\alpha\beta} &= \frac{e\hbar^2}{m\epsilon_{\alpha\beta}^2} \int dV [(H\psi_\alpha^*) \nabla_\mu \psi_\beta - \psi_\alpha^* \nabla_\mu (H\psi_\beta)] E_\mu \\ &= \frac{-e\hbar^4}{2m^2\epsilon_{\alpha\beta}^2} \int dV [(\Delta\psi_\alpha^*) \nabla_\mu \psi_\beta - \psi_\alpha^* \nabla_\mu (\Delta\psi_\beta)] E_\mu. \end{aligned} \quad (\text{A4})$$

Integrating the first term by parts yields the surface contribution

$$M_{\alpha\beta}^s = \frac{-e\hbar^4}{2m^2\epsilon_{\alpha\beta}^2} \int dS_\nu (\nabla_\nu \psi_\alpha^*) E_\mu \nabla_\mu \psi_\beta, \quad (\text{A5})$$

while the rest represents the bulk contribution, which can be manipulated to the form

$$M_{\alpha\beta}^b = \frac{e\hbar^4}{m^2\epsilon_{\alpha\beta}^2} \int dV (\nabla_\mu \psi_\alpha^*) (\nabla_\nu E_\mu) \nabla_\nu \psi_\beta. \quad (\text{A6})$$

Since the local fields change smoothly on the Fermi wavelength scale, the bulk contribution is negligibly small. Noting that only *normal* derivatives of  $\psi_\alpha$  do not vanish at the (hard-wall) boundary  $S$ , the surface contribution to matrix element takes the form

$$M_{\alpha\beta}^s = \frac{-e\hbar^4}{2m^2\epsilon_{\alpha\beta}^2} \int dS [\nabla_n \psi_\alpha(\mathbf{s})]^* E_n(\mathbf{s}) \nabla_n \psi_\beta(\mathbf{s}), \quad (\text{A7})$$

where  $\nabla_n \psi_\alpha(\mathbf{s}) \equiv [\mathbf{n} \cdot \nabla \psi_\alpha(\mathbf{r})]_{\mathbf{r} \rightarrow \mathbf{s}_-}$  is the wave function's normal derivative at the boundary point  $\mathbf{s}$  on the inner side [ $\mathbf{n}(\mathbf{s})$  is the outward normal to the surface at point  $\mathbf{s}$ ] and  $eE_n(\mathbf{s}) = -\nabla_n \Phi(\mathbf{s})$  defines the corresponding normal field component.

## Appendix B: Electron-hole surface correlation function

### 1. Multiple-reflection expansion

The electron Green function in a hard-wall potential well can be presented as an infinite series in reflections from the boundary as (suppressing energy dependence) [72]

$$G(\mathbf{r}, \mathbf{r}') = G_0(\mathbf{r} - \mathbf{r}') - \frac{\hbar^2}{2m} \int dS G_n(\mathbf{r}, \mathbf{s}) G_0(\mathbf{s} - \mathbf{r}'), \quad (\text{B1})$$

where  $G_n(\mathbf{r}, \mathbf{s}) \equiv \nabla_n G(\mathbf{r}, \mathbf{s})$  is the normal derivative of the Green function at surface point  $\mathbf{s}$  on the boundary inner side, satisfying

$$G_n(\mathbf{r}, \mathbf{s}) = 2G_n^0(\mathbf{r} - \mathbf{s}) - \frac{\hbar^2}{m} \int dS' G_{n'}(\mathbf{r}, \mathbf{s}') \bar{G}_n^0(\mathbf{s}' - \mathbf{s}). \quad (\text{B2})$$

Here,  $G_0(\epsilon, r) = (m/2\pi\hbar^2) e^{ik_\epsilon r}/r$ , with  $k_\epsilon = \sqrt{2m\epsilon}/\hbar$ , is the free electron Green function, and

$$\bar{G}_n^0(\mathbf{s}' - \mathbf{s}) = \frac{1}{2} [G_n^0(\mathbf{s}' - \mathbf{s}_+) + G_n^0(\mathbf{s}' - \mathbf{s}_-)] \quad (\text{B3})$$

is its *symmetric* normal derivative at the inner ( $\mathbf{s}_-$ ) and outer ( $\mathbf{s}_+$ ) boundary sides. Iterations of this system lead to the multiple-reflection expansion [72]. For characteristic cavity size  $L \gg \lambda_F$ , the leading contribution comes from the direct and single-reflection paths [first term in Eq. (B2)], while the higher-order terms account for multiple reflections due to the surface curvature  $R \sim L$ , and are suppressed by powers of  $\lambda_F/R$  [72]. Since the Fermi wavelength in metals is small,  $\lambda_F < 1$  nm, the higher-order terms can be disregarded. The equation for  $G_{nn'}(\mathbf{s}, \mathbf{s}')$  is obtained by taking the normal derivative of Eq. (B2). Keeping only the first term, we obtain

$$G_{nn'}(\mathbf{s}, \mathbf{s}') = 2G_{nn'}^0(\mathbf{s} - \mathbf{s}'). \quad (\text{B4})$$

## 2. Evaluation of $\bar{F}_\omega$

To evaluate  $\rho_{nn'}(\epsilon; \mathbf{s}, \mathbf{s}') = 2\text{Im}G_{nn'}^0(\mathbf{s} - \mathbf{s}')$ , we use the fact that the size of characteristic region dominating surface integrals in the correlation function  $F$  is  $|\mathbf{s} - \mathbf{s}'| \sim v_F/\omega \ll L$ , and compute normal derivatives of  $G_0(\mathbf{r} - \mathbf{r}')$  with respect to the tangent plane  $z = 0$ ,

$$\begin{aligned} G_{zz'}(\epsilon, \mathbf{s} - \mathbf{s}') &= 2 \left[ \frac{\partial}{\partial z} \frac{\partial}{\partial z'} G_0(\epsilon, \mathbf{r} - \mathbf{r}') \right]_{z, z'=0} \\ &= -2 \left[ \frac{\partial^2}{\partial z^2} G_0(\epsilon, \mathbf{r} - \mathbf{r}') \right]_{z, z'=0}. \end{aligned} \quad (\text{B5})$$

Introducing notations  $r = \sqrt{s^2 + z^2}$ , we write

$$\frac{\partial^2}{\partial z^2} G_0(\epsilon, r) = \left[ \left( \frac{\partial r}{\partial z} \right)^2 \frac{\partial^2}{\partial r^2} + \frac{\partial^2 r}{\partial z^2} \frac{\partial}{\partial r} \right] G_0(\epsilon, r), \quad (\text{B6})$$

and, in the limit  $z = 0$ , we obtain

$$\left[ \frac{\partial^2}{\partial z^2} G_0(\epsilon, r) \right]_{z=0} = \frac{1}{s} \frac{\partial}{\partial s} G_0(\epsilon, s), \quad (\text{B7})$$

yielding

$$\rho_{zz}(\epsilon, s) = \frac{m}{\pi \hbar^2 s} \frac{\partial}{\partial s} \frac{\sin k_\epsilon s}{s}. \quad (\text{B8})$$

To evaluate  $\bar{F}_\omega$ , we note that for  $L \gg v_F/\omega$ , the surface integral can be replaced by integral over the tangent plane,

$$\begin{aligned} \bar{F}_\omega &= \frac{m^2}{\pi^2 \hbar^4} \int d\epsilon f_\omega(\epsilon) \int \frac{d^2 \mathbf{s}}{s^2} \left[ \frac{\partial}{\partial s} \frac{\sin k_\epsilon s}{s} \right] \left[ \frac{\partial}{\partial s} \frac{\sin k_{\epsilon + \hbar\omega} s}{s} \right] \\ &= \frac{m^2}{4\pi \hbar^4} \int d\epsilon f_\omega(\epsilon) \left[ k_\epsilon k_{\epsilon + \hbar\omega} (k_\epsilon^2 + k_{\epsilon + \hbar\omega}^2) \right. \\ &\quad \left. - (k_{\epsilon + \hbar\omega}^2 - k_\epsilon^2)^2 \text{arctanh} \left( \frac{k_\epsilon}{k_{\epsilon + \hbar\omega}} \right) \right]. \end{aligned} \quad (\text{B9})$$

The function  $f_\omega(\epsilon) = f(\epsilon) - f(\epsilon + \hbar\omega)$  restricts the energy integral to the interval of width  $\hbar\omega$ , and, after rescaling the integration variable, we obtain

$$\bar{F}_\omega = \hbar\omega \frac{2m^4 E_F^2}{\pi \hbar^8} g(\hbar\omega/E_F), \quad (\text{B10})$$

where the function

$$\begin{aligned} g(\xi) &= \int_{-1/2}^{-1/2} dx \left[ (1 + \xi x) \left[ (1 + \xi x)^2 - \frac{\xi^2}{4} \right]^{1/2} \right. \\ &\quad \left. - \xi^2 \text{arctanh} \left[ \frac{1 + \xi(x - 1/2)}{1 + \xi(x + 1/2)} \right] \right]^{1/2} \end{aligned} \quad (\text{B11})$$

is normalized to unity,  $g(0) = 1$ . Then, we obtain

$$Q_s = \frac{e^2}{2\pi^2 \hbar} \frac{E_F^2}{(\hbar\omega)^2} g(\hbar\omega/E_F) \int dS |E_n|^2. \quad (\text{B12})$$

Finally, for optical frequency well below the Fermi energy,  $\hbar\omega/E_F \ll 1$ , and using the relation  $\omega_p^2 = 4\pi e^2 n/m = 4e^2 k_F^3/3\pi m$ , where  $n$  is the electron concentration, we arrive at surface contribution to the absorbed power:

$$Q_s = \frac{3v_F \omega_p^2}{32\pi \omega^2} \int dS |E_n|^2. \quad (\text{B13})$$

## Appendix C: Scattering rate for separable shapes

For system geometries that allow separation of variables, we present the potential as  $\Phi(\mathbf{r}) = R(\xi)\Sigma(\eta, \zeta)$ , where  $\xi$  is the radial (normal) coordinate and the pair  $(\eta, \zeta)$  parametrizes the surface. With surface area element  $dS = h_\eta h_\zeta d\eta d\zeta$  and normal derivative  $\nabla_n = h_\xi^{-1}(\partial/\partial\xi)$ , where  $h_i$  are the scale factors ( $i = \xi, \eta, \zeta$ ), the surface scattering rate takes the form

$$\gamma_s = \frac{3v_F}{4} \frac{R'(\xi)}{R(\xi)} \frac{\int \int d\eta d\zeta (h_\eta h_\zeta / h_\xi^2) |\Sigma|^2}{\int \int d\eta d\zeta (h_\eta h_\zeta / h_\xi) |\Sigma|^2}. \quad (\text{C1})$$

Below we evaluate  $\gamma_s$  for a spheroidal particle.

Spheroidal metal nanoparticles exhibit longitudinal and transverse plasmon modes with electric field oscillating, respectively, along the axis of symmetry (semiaxis  $a$ ) and within the symmetry plane (semiaxis  $b$ ). Inside the prolate spheroid ( $b/a < 1$ ), the potential has the form  $\Phi_n(\mathbf{r}) \propto P_l^{|m|}(\xi) Y_{lm}(\eta, \phi)$ , where  $P_l^m(x)$  is the Legendre function of the first kind. Spheroid surface corresponds to  $\xi = a/f$  where  $f = \sqrt{a^2 - b^2}$  is half the distance between the foci, and the scale factors are given by

$$\begin{aligned} h_\xi &= f \sqrt{\frac{\xi^2 - \eta^2}{\xi^2 - 1}}, \quad h_\eta = f \sqrt{\frac{\xi^2 - \eta^2}{1 - \eta^2}}, \\ h_\phi &= f \sqrt{(\xi^2 - 1)(1 - \eta^2)}. \end{aligned} \quad (\text{C2})$$

The surface area and volume of the prolate spheroid are

$$S = 2\pi \left( b^2 + \frac{ab\alpha}{\sin\alpha} \right), \quad V = \frac{4\pi}{3} b^2 a, \quad (\text{C3})$$

where  $\alpha = \arccos(b/a)$  is the angular eccentricity. A straightforward evaluation of Eq. (C1) yields:

$$\begin{aligned} \gamma_s^{lm} &= \frac{3v_F}{4f} \frac{(2l+1)!(l-|m|)!}{2(l+|m|)!} \\ &\quad \times \frac{[P_l^{|m|}(\xi)]'}{P_l^{|m|}(\xi)} \sqrt{\xi^2 - 1} \int_{-1}^1 d\eta \frac{[P_l^{|m|}(\eta)]^2}{\sqrt{\xi^2 - \eta^2}}. \end{aligned} \quad (\text{C4})$$

For longitudinal and transverse *dipole* modes, i.e.,  $(lm) = (10)$  and  $(lm) = (11)$ , respectively, we obtain  $\gamma_s^{L,T} = (3v_F/4a)f_{L,T}$ , where

$$f_L = \frac{3}{2 \tan^2 \alpha} \left[ \frac{2\alpha}{\sin 2\alpha} - 1 \right], \quad f_T = \frac{3}{4 \sin^2 \alpha} \left[ 1 - \frac{2\alpha}{\tan 2\alpha} \right], \quad (\text{C5})$$

are the normalized (to spherical shape) rates. Within the CS model, the decay rate has the form  $\gamma_{cs} = v_F S/4V =$

$(3v_F/4a)f_{cs}$ , where

$$f_{cs} = \frac{aS}{3V} = \frac{1}{2} \left[ 1 + \frac{2\alpha}{\sin 2\alpha} \right]. \quad (\text{C6})$$

The rates for the oblate spheroid ( $b/a > 1$ ) are described by the above expressions with  $\alpha = i \operatorname{arccosh}(b/a)$ .

- 
- [1] S. A. Maier and H. A. Atwater, *J. Appl. Phys.* **98**, 011101 (2005).
- [2] E. Ozbay, *Science* **311**, 189 (2006).
- [3] M. I. Stockman, in *Plasmonics: Theory and Applications*, edited by T. V. Shahbazyan and M. I. Stockman (Springer, New York, 2013).
- [4] E. C. Le Ru and P. G. Etchegoin, *Principles of Surface-Enhanced Raman Spectroscopy* (Elsevier, Amsterdam, 2009).
- [5] L. Novotny and B. Hecht, *Principles of Nano-Optics* (CUP, New York, 2012).
- [6] D. J. Bergman and M. I. Stockman, *Phys. Rev. Lett.* **90**, 027402 (2003).
- [7] J. R. Lakowicz, *Anal. Biochem.* **298**, 1 (2001).
- [8] J. Zhao, X. Zhang, C. Yonzon, A. J. Haes, and R. P. Van Duyne, *Nanomedicine* **1**, 219 (2006).
- [9] H. A. Atwater and A. Polman, *Nat. Mater.* **9**, 205 (2010).
- [10] M. L. Brongersma, N. J. Halas, and P. Nordlander, *Nat. Nanotechnol.* **10**, 25 (2015).
- [11] W. P. Halperin, *Rev. Mod. Phys.* **58**, 533 (1986).
- [12] V. V. Kresin, *Phys. Rep.* **220**, 1 (1992).
- [13] C. Voisin, N. Del Fatti, D. Christofilos, and F. Vallée, *J. Phys. Chem. B* **105**, 2264 (2001).
- [14] K. L. Kelly, E. Coronado, L. L. Zhao, and G. C. Schatz, *J. Phys. Chem. B* **107** 668 (2003).
- [15] C. Noguez, *J. Phys. Chem. C* **111** 3806 (2007).
- [16] A. Wokaun, J. P. Gordon, and P. F. Liao, *Phys. Rev. Lett.* **48**, 957 (1982).
- [17] U. Kreibig and M. Vollmer, *Optical Properties of Metal Clusters* (Springer, Berlin, 1995).
- [18] Y. K. Lee, C. H. Jung, J. Park, H. Seo, G. A. Somorjai, and J. Y. Park, *Nano Lett.* **11**, 4251 (2011).
- [19] F. Wang and N. A. Melosh, *Nano Lett.* **11**, 5426 (2011).
- [20] M. W. Knight, H. Sobhani, P. Nordlander, and N. J. Halas, *Science* **332**, 702 (2011).
- [21] A. Sobhani, M. W. Knight, Y. Wang, B. Zheng, N. S. King, L. V. Brown, Z. Fang, P. Nordlander, and N. J. Halas, *Nat. Commun.* **4**, 1643 (2013).
- [22] K. Wu, W. E. Rodriguez-Cordoba, Y. Yang, and T. Lian, *Nano Lett.* **13**, 5255 (2013).
- [23] M. W. Knight, Y. Wang, A. S. Urban, A. Sobhani, B. Y. Zheng, P. Nordlander, and N. J. Halas, *Nano Lett.* **13**, 1687 (2013).
- [24] C. Clavero, *Nat. Photonics* **8**, 95 (2014).
- [25] H. Chalabi, D. Schoen, M. L. Brongersma, *Nano Lett.* **14**, 1374 (2014).
- [26] R. Sundararaman, P. Narang, A. S. Jermyn, W. A. Goddard III, and H. A. Atwater, *Nat. Commun.* **5**, 5788 (2014).
- [27] B. Y. Zheng, H. Zhao, A. Manjavacas, M. McClain, P. Nordlander, and N. J. Halas, *Nat. Commun.* **6**, 7797 (2015).
- [28] I. Thomann, B. A. Pinaud, Z. Chen, B. M. Clemens, T. F. Jaramillo, and M. L. Brongersma, *Nano Lett.* **11**, 3440 (2011).
- [29] J. Lee, S. Mubeen, X. Ji, G. D. Stucky, and M. Moskovits, *Nano Lett.* **12**, 5014 (2012).
- [30] S. Mukherjee, F. Libisch, N. Large, O. Neumann, L. V. Brown, J. Cheng, J. B. Lassiter, E. A. Carter, P. Nordlander, and N. J. Halas, *Nano Lett.* **13**, 240 (2013).
- [31] S. Mubeen, J. Lee, N. Singh, S. Krämer, G. D. Stucky, and M. Moskovits, *Nat. Nanotechnol.* **8**, 247 (2013).
- [32] S. Mukherjee, L. Zhou, A. M. Goodman, N. Large, C. Ayala-Orozco, Y. Zhang, P. Nordlander, and N. J. Halas, *J. Am. Chem. Soc.* **136**, 64 (2014).
- [33] T. Klar, M. Perner, S. Grosse, G. von Plessen, W. Spirkl, and J. Feldmann, *Phys. Rev. Lett.* **80**, 4249 (1998).
- [34] C. Sönnichsen, T. Franzl, T. Wilk, G. von Plessen, J. Feldmann, O. V. Wilson, and P. Mulvaney, *Phys. Rev. Lett.* **88**, 077402 (2002).
- [35] S. L. Westcott, J. B. Jackson, C. Radloff, and N. J. Halas, *Phys. Rev. B* **66**, 155431 (2002).
- [36] G. Raschke, S. Brogl, A. S. Susha, A. L. Rogach, T. A. Klar, and J. Feldmann, *Nano Lett.* **4**, 1853 (2004).
- [37] A. Arbouet, D. Christofilos, N. Del Fatti, F. Vallée, J. R. Huntzinger, L. Arnaud, P. Billaud, and M. Broyer, *Phys. Rev. Lett.* **93**, 127401 (2004).
- [38] C. L. Nehl, N. K. Grady, G. P. Goodrich, F. Tam, N. J. Halas, and J. H. Hafner, *Nano Lett.* **4**, 2355 (2004).
- [39] C. Novo, D. Gomez, J. Perez-Juste, Z. Zhang, H. Petrova, M. Reismann, P. Mulvaney, and G. V. Hartland, *Phys. Chem. Chem. Phys.* **8**, 3540 (2006).
- [40] H. Baida, P. Billaud, S. Marhaba, D. Christofilos, E. Cottancin, A. Crut, J. Lermé, P. Maioli, M. Pellarin, M. Broyer, N. Del Fatti, and F. Vallée, *Nano Lett.* **9**, 3463 (2009).
- [41] M. G. Blaber, A.-I. Henry, J. M. Bingham, G. C. Schatz, and R. P. Van Duyne, *J. Phys. Chem. C* **116**, 393 (2012).
- [42] V. Juvé, M. F. Cardinal, A. Lombardi, A. Crut, P. Maioli, J. Pérez-Juste, L. M. Liz-Marzán, N. Del Fatti, and F. Vallée, *Nano Lett.* **13**, 2234 (2013).
- [43] M. N. O'Brien, M. R. Jones, K. L. Kohlstedt, G. C. Schatz, and C. A. Mirkin, *Nano Lett.* **15**, 1012 (2015).
- [44] A. Kawabata and R. Kubo, *J. Phys. Soc. Jpn.* **21**, 1765 (1966).
- [45] A. A. Lushnikov and A. J. Simonov, *Z. Physik* **270**, 17 (1974).
- [46] W. A. Kraus and G. C. Schatz, *J. Chem. Phys.* **79**, 6130 (1983).
- [47] M. Barma and V. J. Subrahmanyam, *J. Phys.: Cond. Mat.* **1**, 7681 (1989).
- [48] C. Yannouleas and R. A. Broglia, *Ann. Phys.* **217**, 105 (1992).
- [49] M. Eto and K. Kawamura, *Surf. Rev. Lett.* **3**, 151 (1996).

- [50] A. V. Uskov, I. E. Protsenko, N. A. Mortensen, and E. P. O'Reilly, *Plasmonics* **9**, 185 (2013).
- [51] J. B. Khurgin and G. Sun, *Opt. Express* **23**, 250905 (2015).
- [52] R. A. Molina, D. Weinmann, and R. A. Jalabert, *Phys. Rev. B* **65**, 155427 (2002).
- [53] G. Weick, R. A. Molina, D. Weinmann, and R. A. Jalabert, *Phys. Rev. B* **72**, 115410 (2005).
- [54] Z. Yuan and S. Gao, *Surf. Sci.* **602**, 460 (2008).
- [55] J. Lermé, H. Baida, C. Bonnet, M. Broyer, E. Cottancin, A. Crut, P. Maioli, N. Del Fatti, F. Vallée, and M. Pellarin, *J. Phys. Chem. Lett.* **1**, 2922 (2010).
- [56] J. Lermé, *J. Phys. Chem. C* **115**, 14098 (2011).
- [57] X. Li, Di Xiao, and Z. Zhang, *New J. Phys.* **15**, 023011 (2013).
- [58] A. Manjavacas, J. G. Liu, V. Kulkarni, and P. Nordlander, *ACS Nano* **8**, 7630 (2014).
- [59] T. Christensen, W. Yan, A.-P. Jauho, M. Soljačić, and N. A. Mortensen, arXiv:1608.05421.
- [60] N. A. Mortensen, *Photonic. Nanostruct.* **11**, 303 (2013).
- [61] N. A. Mortensen, S. Raza, M. Wubs, T. Søndergaard, and S. I. Bozhevolnyi, *Nat. Commun.* **5**, 3809 (2014).
- [62] L. Genzel, T. P. Martin, and U. Kreibig, *Z. Phys. B* **21**, 339 (1975).
- [63] R. Ruppin and H. Yatom, *Phys. Status Solidi* **74**, 647 (1976).
- [64] W. A. Krauss and G. C. Schatz, *Chem. Phys. Lett.* **99**, 353 (1983).
- [65] E. A. Coronado and G. C. Schatz, *J. Chem. Phys.* **119**, 3926 (2003).
- [66] A. Moroz, *J. Phys. Chem. C* **112**, 10641 (2008).
- [67] J. A. Scholl, A. L. Koh, J. A. Dionne, *Nature (London)* **483**, 421 (2012).
- [68] A. S. Kirakosyan, M. I. Stockman, and T. V. Shahbazyan, *Phys. Rev. B* **94**, 155429 (2016).
- [69] T. V. Shahbazyan, *Phys. Rev. Lett.* **117**, 207401 (2016).
- [70] L. D. Landau and E. M. Lifshitz, *Electrodynamics of Continuous Media* (Elsevier, Amsterdam, 2004).
- [71] G. D. Mahan, *Many-Particle Physics* (Plenum, New York, 1990).
- [72] R. Balian and C. Bloch, *Ann. Phys.* **60**, 401 (1970).
- [73] V. N. Pustovit and T. V. Shahbazyan, *Phys. Rev. B* **73**, 085408 (2006).